DOI 10.24425/aee.2026.158264

Development of a primary frequency regulation capability evaluation index for wind-solar-storage systems based on the entropy weight method

CONGSHAN LI ✉, JIAHAO GAO, PING HE, YUQI JI, HANG WEI

College of Electrical and Information Engineering
Zhengzhou University of Light Industry
450002 Zhengzhou China

e-mail: ✉ *2015018@zzuli.edu.cn*

(Received: 25.11.2025, revised: 28.04.2026)

Abstract: With the deepening of the construction of the new power system, the penetration rate of new energy in the power system continues to increase significantly. However, the traditional assessment of the ability of new energy (wind, solar, and storage) to participate in the primary frequency response (PFR) of the system exhibits limitations due to the difficulty in fully considering their differentiated characteristics. Therefore, this study develops a comprehensive evaluation index system for the PFR performance of wind-solar-storage new energy systems based on the entropy weight method. This system fully incorporates the characteristics of wind power generation, photovoltaic power generation, and energy storage systems in terms of frequency response and operational constraints, establishing overall PFR capability evaluation indicators of the system, as well as specialized and refined evaluation indicators for each technology. Simulation results demonstrated the methodology's effectiveness, demonstrating its capability to accurately assess frequency regulation capacities while considering the distinct operational characteristics of wind, solar, and storage technologies. These findings provide theoretical guidance for optimizing frequency regulation resource allocation and operational strategies in renewable-dominated power systems.

Key words: entropy weight method, frequency regulation capability evaluation, index system, new energy, primary frequency regulation

1. Introduction

The rapid expansion of wind and solar power has made high-penetration renewable integration a dominant trend in global power system development [1]. However, this transition poses critical challenges to grid frequency stability: converter-interfaced renewable generation systems (wind turbines, photovoltaic arrays, and energy storage units) inherently exhibit weaker frequency regulation capability and lower rotational inertia than conventional synchronous generators [2]. As renewables displace traditional synchronous generation, power systems experience a progressive decline in rotational inertia and natural frequency stabilization capacity [3]. This risk is further exacerbated by the inherent intermittency and volatility of renewable sources, which drive frequent active power fluctuations and increase the likelihood of frequency instability events [4].

With the increasing penetration of renewable energy in modern power grids, renewable energy sources such as wind, solar photovoltaic (PV), and pumped hydro storage units have been widely adopted for grid frequency support [5]. As renewable energy systems increasingly participate in primary frequency regulation (PFR), the limitations of existing evaluation methods for wind-solar-storage systems' PFR performance have become increasingly prominent. Wind and solar stations provide frequency support mainly through grid-connected converter control adjustment, active power reserve, and coordinated operation with integrated energy storage systems [6]. However, unlike synchronous generators with fixed frequency regulation characteristics, renewable energy systems exhibit significant variability in frequency regulation capability due to changing environmental conditions and real-time operating states, whereas the capacity and dynamic response characteristics of energy storage systems also significantly impact their frequency regulation performance [7]. Developing a scientific frequency regulation assessment framework for high renewable penetration scenarios is critical for two core purposes: 1) to fully tap the frequency support potential of renewable stations and ensure grid dynamic stability; 2) to establish data-driven benchmarks for power system regulation and dispatching decisions.

Substantial research has focused on assessing the frequency regulation capabilities of conventional synchronous generators. Reference [8] proposed an algorithm with differentiated integration weights for PFR contribution evaluation, which can effectively capture the sensitivity of generating units to frequency variations. Reference [9] developed a SWOT-based framework (Strengths, Weaknesses, Opportunities, and Threats) integrating internal and external evaluation factors to assess the operational security of renewable energy power systems in China, and adopted a fuzzy analytic hierarchy process (AHP) method to assign weights to each evaluation element. Reference [10] investigated the PFR evaluation index system for thermal power units, established principal and auxiliary evaluation indices based on classical dynamic performance indicators, and clarified corresponding performance benchmarks and assessment criteria. Reference [11] designed a prediction method for power system primary frequency regulation capability based on Mind Evolutionary Al-gorithm (MEA) neural network, which takes ten characteristic variables including system frequency, load level, active power and power deficit as inputs, to forecast the dynamic power compensation trajectory within the 60-second window after grid disturbance. However, current research mainly focuses on PFR capability evaluation for conventional power systems, and lacks a dedicated assessment methodology tailored for high-penetration renewable energy integrated power systems.

Given the fundamental differences in frequency regulation mechanisms between renewable energy power plants and conventional synchronous generators, their dynamic response patterns, power fluctuation characteristics and control flexibility have a decisive impact on the frequency stability boundary of high-renewable power systems. In this context, scholars have carried out extensive exploratory research on renewable energy frequency regulation performance evaluation. Reference [12] defined key performance indicators for frequency stability assessment in converter-dominated power systems, and mapped system operational variables to stability metrics through actual field operation data. Reference [13] analyzed the development landscape of renewable energy in China and the control methodologies for conventional and renewable generation, and proposed frequency response evaluation indices covering inertial response metrics and PFR evaluation indicators. Reference [14] established performance evaluation standards for energy storage active power control in multi-region power grids, providing guidance for the optimization of energy storage frequency regulation control strategies. Reference [15] developed a dual-indicator system to evaluate the static and dynamic primary frequency regulation ability (PFRA) of renewable power stations. Reference [16] implemented a multi-criteria assessment of frequency regulation performance for pumped storage plants in isolated power systems. Reference [17] proposed a wind turbine frequency regulation capability assessment methodology based on operational status analysis, and defined energy and power margin coefficients to quantify support potential. Reference [18] constructed a comprehensive evaluation system for wind-storage hybrid frequency regulation systems, integrating frequency deviation metrics with economic factors, and proposed an optimal control strategy for wind-storage systems. Reference [19] established a three-dimensional evaluation architecture covering frequency stability, power support and power regulation capability, and developed an integrated assessment model for photovoltaic plant frequency regulation. Reference [20] systematically categorized the key operational parameters of energy storage systems for frequency regulation scenarios. However, existing studies still have two key limitations. Most works focus on the frequency regulation performance of individual components in renewable energy systems (e.g., standalone wind turbines, photovoltaic plants, or energy storage units), and lack a holistic evaluation framework for the overall frequency regulation capability of integrated wind-solar-storage hybrid systems. Meanwhile, few studies have systematically analyzed the inherent differences in frequency regulation characteristics among wind, photovoltaic and energy storage subsystems, leading to poor applicability of existing evaluation methods in practical wind-solar-storage integrated projects.

To fill the above research gaps, this study develops a multi-criteria PFR capability evaluation framework for wind-solar-storage hybrid systems based on the entropy weight method. First, the frequency regulation mechanisms of wind farms, photovoltaic plants, and battery energy storage systems are systematically analyzed, and a novel multi-dimensional evaluation index system is constructed to fully characterize the core frequency regulation characteristics of each type of resource. Then, the entropy weight method is adopted to calculate the objective weight of each evaluation index, which avoids the subjectivity of traditional empirical weighting, and a quantitative evaluation system for wind-solar-storage system PFR capability is established. The proposed framework can provide critical technical reference for optimal grid dispatching of renewable energy frequency regulation resources. Finally, a coordinated frequency regulation simulation platform for wind-solar-storage integrated systems is built in MATLAB/Simulink, and multiple sets of simulation cases are carried out to verify the effectiveness and rationality of the proposed evaluation method.

2. New energy frequency modulation principle analysis

Droop control and power reserve control represented two widely adopted approaches for renewable energy systems and energy storage to provide primary frequency regulation in power grids. This study employed droop control to regulate power output across renewable generation and storage units, while power reserve control was implemented to ensure upward reserve availability from wind/PV systems, with an adaptive droop coefficient adjustment mechanism was implemented to safeguard energy storage systems against over-charge/discharge cycles during PFR events.

The wind-solar-storage energy systems architecture shown in Fig. 1 was comprised of wind turbines, PV arrays, and battery energy storage systems (BESSs) within the renewable energy station. Each generation/storage unit is interconnected through power converters to a common AC bus, which was interfaced with a synchronous generator via a transformer. Loads were connected at both the generator-side and bus-side terminals of the transformer.

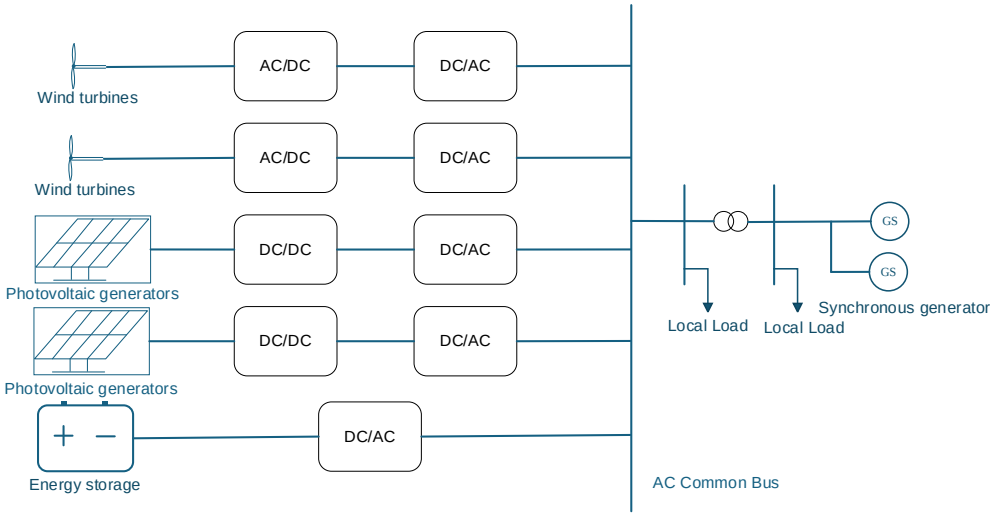

Fig. 1. Structural diagram of novel power system with wind–solar–storage integration

2.1. Wind power load shedding primary frequency regulation

Under maximum power point tracking (MPPT) mode (below rated wind speed) and constant power mode (above rated speed), wind turbines can only provide short-term frequency support through rotor-stored kinetic energy, which cannot support sustained PFR energy delivery [21]. To enable sustained PFR capability, power reserve control with capacity reserve is required. Under stable wind conditions, active power regulation was achieved through coordinated rotor speed variation and pitch angle adjustments [22].

Wind power captured by wind turbines P_m is calculation as:

$$P_m = \frac{1}{2} C_p(\lambda, \beta) \rho A v^3, \tag{1}$$

where: ρ is the air density, A is the rotor swept area, v is the wind speed, $C_p\ (\lambda, \beta)$ is the power coefficient, λ is the tip-speed ratio, and β is the pitch angle.

This study implemented an over-speed control to enable sustained frequency support capability in wind turbines. The control architecture dynamically adjusted rotor speed by modifying the rotor-side converter, thereby achieving real-time power regulation for grid frequency stabilization through active power modulation.

$$\Delta P_w = -K_w \Delta f, \tag{2}$$

where: ΔP_w is the variation in the wind turbine's PFR reference value, K_w is the droop coefficient of the wind turbine, and Δf is the grid frequency deviation.

2.2. Photovoltaic load shedding primary frequency regulation

Unlike wind turbines and synchronous generators, photovoltaic systems lack rotating mechanical components and exhibit negligible equivalent inertia due to limited energy storage in DC-link capacitors. This inherent characteristic necessitates power reserve control to enable PFR capability.

The photovoltaic array Voltage–Power curve is shown in Fig. 2. In this paper, the PV array voltage was controlled to be higher than the MPPT level when the frequency is stable, so that the power of the PV power plant is lower than the maximum power, and the ability to participate in the primary frequency regulation was obtained.

$$\Delta P_{\mathrm{pv}} = -K_{\mathrm{pv}} \Delta f, \tag{3}$$

where ΔP_{pv} represents the variation in the PV array's PFR reference value and K_{pv} is the droop coefficient of the PV array.

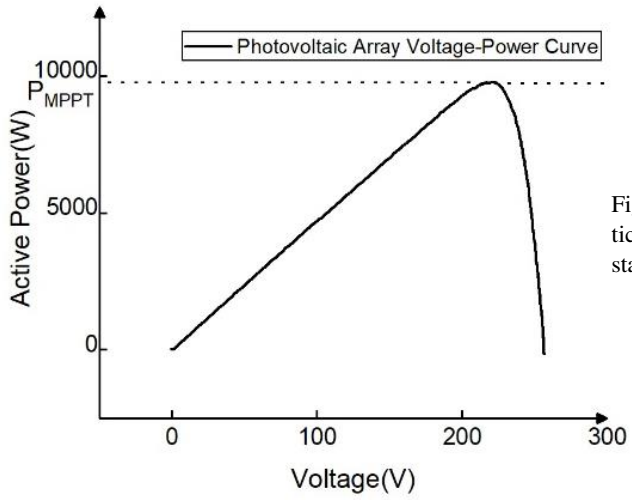

Fig. 2. Voltage–power (P–V) characteristic curve of the photovoltaic array under standard test conditions (STC: irradiance 1000 W/m^2, cell temperature 25°C)

2.3. Energy storage adaptive primary frequency regulation

Battery energy storage has four-quadrant regulation capability, high operational flexibility, and can provide fast active power support for the system in the initial stage of frequency deviation, giving it broad application prospects in grid frequency support.

The battery energy storage system through the DC/AC grid-connected converter controls energy storage system output power to support the system frequency stability, energy storage response to frequency deviation in the more widely used control methods for active power frequency droop control strategy, and amount of active changes, as shown in Equation 4.

$$\Delta P_{\text{ess}} = -K_{\text{ess}}\Delta f, \tag{4}$$

where ΔP_{ess} is the variation in energy storage system's PFR reference value and K_{ess} is the droop coefficient of the energy storage system.

Energy storage droop control strategies were categorized into fixed K_{ess} and variable K_{ess} approaches. While the former offers simpler implementation, its constant droop coefficient may induce excessive or insufficient energy storage capacity during prolonged load variations, compromising battery lifespan and system flexibility. To simultaneously optimize energy storage capacity and primary frequency regulation efficacy, this study employed an adaptive droop control strategy for BESSs. This method calculated K_{ess} values through a hyperbolic tangent function [23], effectively maintaining energy storage capacity within an optimal operational range. The proposed parameter configuration and control methodology demonstrate relative simplicity, when the battery is discharged:

$$K_b = K_{B\max}\left(\frac{\exp[n(S_{\text{SOC}} - S_{\text{mid}})]}{\exp[n(S_{\text{SOC}} - S_{\text{mid}})] + 1}\right). \tag{5}$$

When the battery is charging:

$$K_b = K_{B\max}\left(\frac{1 - \exp[n(S_{\text{SOC}} - S_{\text{mid}})]}{1 + \exp[n(S_{\text{SOC}} - S_{\text{mid}})]}\right), \tag{6}$$

where: $K_{B\max}$ is the set maximum droop coefficient, S_{soc} is the state of charge (SOC) of the energy storage system, and S_{mid} is the midpoint value within the predefined upper and lower S_{soc}. The parameter n exhibits a proportional relationship with the magnitude of K_b near this midpoint, enabling significant power output variations within narrow S_{soc} ranges through amplified K_b adjustments.

3. A quantitative evaluation framework for primary frequency regulation

3.1. Framework for frequency regulation capability evaluation

Based on the participation mechanisms and regulatory impacts of various components in power system frequency modulation, this study systematically evaluated the frequency stability influences of wind power, photovoltaic generation, and energy storage outputs. A comprehensive assessment framework for the frequency regulation capability of wind-PV-storage integrated systems is developed, the structure of which is illustrated in Fig. 3.

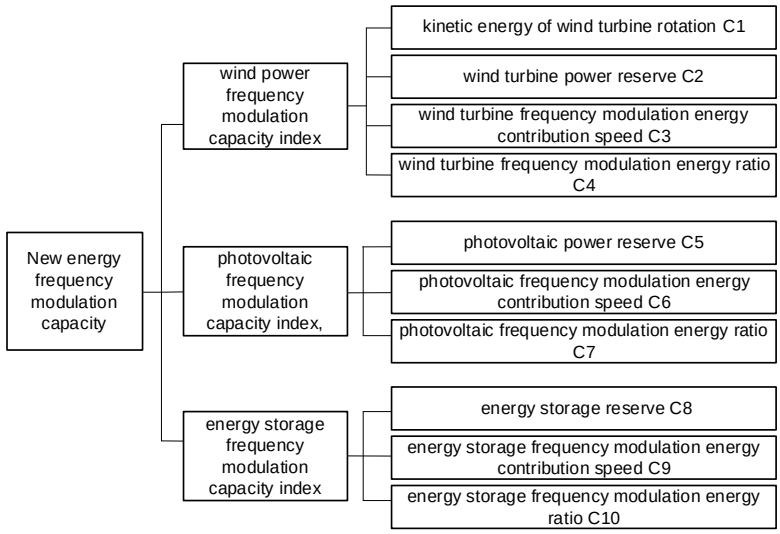

Fig. 3. Framework for frequency modulation capability evaluation system

3.2. Kinetic energy of wind turbine rotation (C1)

Direct-driven wind turbines contribute to frequency regulation through kinetic energy and de-loading. During frequency deviations, these generators modulate rotational speed to absorb or release rotational kinetic energy, thereby mitigating power system fluctuations and enhancing frequency stability. Compared to droop control strategies, rotational kinetic energy provides faster response capabilities, playing a critical role in the initial phase of frequency support.

The rotor kinetic energy exchanged by the generator (C1) is calculated using Eq. 7.

$$C_1 = \frac{1}{2} J_T |\omega_0^2 - \omega_1^2|, \tag{7}$$

where ω_0 denotes the initial rotational speed of the wind turbine before the frequency disturbance and ω_1 denotes the rotational speed after the frequency modulation. J_T is the generator inertia.

3.3. Energy storage reserve (C8)

During frequency regulation processes in wind-PV-storage integrated stations, the energy storage system's PFR output requires continuous SOC monitoring to prevent overcharging/discharging, while ensuring sufficient battery capacity for reliable frequency regulation constitutes a critical operational constraint. This metric functions as a cost indicator when system frequency rises and transitions to a benefit indicator when frequency declines. The energy storage reserve (C8) can be determined as shown in Equation 8.

$$C_8 = (S_{\text{soc}} - S_{\text{soc,min}}) E_B, \tag{8}$$

where: S_{soc} is the SOC of the energy storage, $S_{\text{soc,min}}$ is the minimum allowable SOC, and E_B refers to the rated capacity of energy storage system.

3.4. Wind turbine/photovoltaic power reserve (C2/C5)

Wind turbine/photovoltaic power reserve (C2/C5) represents the adjustable power reserve derived from the difference between the maximum generation capacity and actual output power of renewable energy stations, reflecting the upward regulation potential available from wind turbines and photovoltaic systems during operational states to enhance grid flexibility.

$$C_2 = P_{\mathrm{w,max}} - P_{\mathrm{w,act}}, \tag{9}$$

$$C_5 = P_{\mathrm{pv,max}} - P_{\mathrm{pv,act}}, \tag{10}$$

where $P_{\mathrm{w,max}}$ is the maximum available power of the wind turbine under the current wind speed and $P_{\mathrm{w,act}}$ is the actual operating power of the wind turbine under de-loading operation. $P_{\mathrm{pv,max}}$ is the maximum available power of the photovoltaic array under the current irradiance and temperature and $P_{\mathrm{pv,act}}$ is the actual operating power of the photovoltaic system under de-loading operation.

By maintaining power reserve, wind turbines can rapidly respond to grid frequency deviations through power ramp-up adjustments. This capability substantially improves their participation flexibility in primary frequency regulation, thereby enhancing overall power system adaptability. Similarly, photovoltaic systems achieve de-loading control by operating PV arrays at voltages above or below the MPPT voltage. However, excessive load shedding may compromise downward regulation capability, necessitating its classification as a cost-type metrics during frequency rise events. The power reserve of wind turbines and PV systems fundamentally determine their PFR participation potential, directly influencing the system's frequency regulation performance metrics.

3.5. Frequency modulation energy contribution speed (C3/C6/C9)

The speed of primary frequency regulation fundamentally determines the frequency support capabilities of renewable energy units. System response speed quantifies the temporal effectiveness of power adjustments during frequency deviations, where superior response speed enables faster power modulation to counteract frequency variations. Timely energy delivery during the initial frequency regulation phase is critical, as delayed power contributions – even with adequate terminal energy output – fail to effectively mitigate early-stage frequency fluctuations. This temporal sensitivity necessitates the establishment of a frequency modulation energy contribution speed index, specifically designed to evaluate energy delivery performance during the crucial initial regulation period.

Frequency modulation energy contribution speed (C3/C6/C9) was mathematically defined as:

$$\begin{cases} C_3 = \dfrac{\int_{t_0}^{t_m} \Delta P_w(t)\mathrm{d}t}{t_m - t_0} \\ C_6 = \dfrac{\int_{t_0}^{t_m} \Delta P_{\mathrm{pv}}(t)\mathrm{d}t}{t_m - t_0} \\ C_9 = \dfrac{\int_{t_0}^{t_m} \Delta P_{\mathrm{ess}}(t)\mathrm{d}t}{t_m - t_0} \end{cases}, \tag{11}$$

where: ΔP_w, ΔP_{pv}, ΔP_{ess} represent the power variation magnitude of the wind-solar-storage energy systems, t_0 denotes the initiation timestamp, and t_m indicates the predetermined evaluation endpoint.

3.6. Frequency modulation energy ratio (C4/C7/C10)

During primary frequency regulation processes, frequency regulation resources allocate power imbalance through coordinated responses to both frequency deviation magnitude and speed inequality. However, renewable energy systems frequently deviate from set power due to inherent limitations including frequency regulation dead zones, control system precision errors, and output saturation constraints. The regulation effectiveness correlates positively with the proximity between actual delivered energy and theoretical reference values. This study refers to the frequency regulation energy ratio concept from established grid code specifications "two detailed rules" [24], defining this metric as the proportion between actual frequency regulation energy output and its theoretical maximum, which serves as a critical performance indicator for renewable energy participation in frequency regulation services. The calculation of the indicators is as shown in Formulas (12) and (13).When calculating the wind turbine frequency modulation energy ratio (C_4), the rotor kinetic energy variation induced by rotational speed changes during PFR participation is deducted from the total PFR energy contribution.

$$\begin{cases} C_4 = \dfrac{E_{w,\text{a}} - \frac{1}{2} J_T \left|\omega_0^2 - \omega_m^2\right|}{E_{w,\text{b}}} \\ C_7 = \dfrac{E_{\text{pv},a}}{E_{\text{pv},b}} \\ C_{10} = \dfrac{E_{\text{ess},a}}{E_{\text{ess},b}} \end{cases}, \tag{12}$$

$$\begin{aligned} E_{k,a} &= \int_{t_0}^{t_m} \max\left\{\Delta P_e\left(t\right), 0\right\} \mathrm{d}t \\ E_{k,b} &= \int_{t_0}^{t_m} \max\left\{\Delta P_b\left(t\right), 0\right\} \mathrm{d}t \end{aligned}, \quad k = \{w, \text{pv}, \text{ess}\}, \tag{13}$$

where: $E_{k,a}$ is the actual PFR energy; $E_{k,b}$ is the theoretical PFR energy, σ is the speed inequality, and ΔP_b is the theoretical power variation reference. ΔP_e is the actual power adjustment and ω_m is the initial wind turbine speed.

It should be noted that the energy storage module in this study operates with a variable droop coefficient during the frequency regulation process. Considering that the influence of the SOC on the storage power output has already been represented by the C8 energy storage reserve indicator, the theoretical frequency regulation energy E_b of the storage system is, therefore, calculated with the corresponding variable droop coefficient K_b.

The proposed architecture consists of three primary indicators, which are supported by ten secondary indicators (C1–C10). The wind power frequency modulation capacity index contained four secondary indicators: kinetic energy of wind turbine rotation C1, wind turbine power reserve C2, wind turbine frequency modulation energy contribution speed C3, and wind turbine frequency

modulation energy ratio C4. The photovoltaic frequency modulation capacity index contains three secondary indicators: photovoltaic power reserve C5, photovoltaic frequency modulation energy contribution speed C6, and photovoltaic frequency modulation energy ratio C7; and the energy storage frequency modulation capacity index contains three secondary indicators: energy storage reserve C8, energy storage frequency modulation energy contribution speed C9, and energy storage frequency modulation energy ratio C10. Notably, indicators C2, C5, and C8 were classified as cost-type metrics during frequency increases but were treated as benefit-type metrics during frequency decreases, while all remaining indicators constituted benefit-type metrics.

3.7. Hierarchical design of an informationally independent indicator system

The core objective of this study is to evaluate the absolute PFR hard support capability of wind-solar-storage systems from the perspective of grid dispatching. The indicator system is constructed with absolute physical quantity indicators as the core, to evaluate the absolute primary frequency regulation support capability of wind-PV-storage hybrid systems. Three dimensionless relative indicators (C4, C7, C10) are supplemented to evaluate the utilization efficiency of frequency regulation potential, namely the quality of frequency regulation. Compared with standard single-dimensional dynamic frequency metrics, the constructed aggregated index realizes three core values: comprehensive full-cycle evaluation of frequency regulation performance covering reserve capability, response speed and response accuracy; dual-layer assessment of overall system performance and sub-system contribution positioning; and quantitative decision support for optimal allocation of frequency regulation resources in practical engineering.

To avoid information redundancy and overlapping between indicators, the proposed system is designed following the hierarchical logic of inter-group complete decoupling + intra-group dimensional complementarity, which fully guarantees the informational independence of all indicators. For inter-group indicators, the wind turbine (C1–C4), photovoltaic (C5–C7) and energy storage (C8–C10) indicator groups correspond to three types of frequency regulation resources with completely independent physical mechanisms, with no overlapping calculation basis or information connotation between groups. For intra-group indicators, indicators in the same group characterize frequency regulation performance from mutually independent dimensions including reserve potential, dynamic response speed and utilization efficiency, each with exclusive physical meaning and no redundant reflection of the same frequency regulation information.

4. Weight assignment and comprehensive indicator calculation for primary frequency regulation

Indicator weighting determination typically involves two principal methodologies: subjective assignment based on expert judgment, and objective assignment derived from quantitative analysis of indicator relationships. While subjective methods introduce human experiential insights, objective approaches systematically quantify indicator significance through statistical properties, effectively mitigating subjective bias. This study employs the entropy weight method for PFR indicator weighting, leveraging quantitative assessment of data variability to establish rational weight coefficients.

Entropy is a quantity that characterises the degree of chaos of a system, and entropy weight method is a method to determine the weights of indicators through the entropy value that represents the degree of chaos. In PFR capability evaluation, this method interprets indicator weight significance through data dispersion analysis: higher data variability indicates stronger systemic influence, warranting elevated weighting.

For an evaluation system containing m operational scenarios and n PFR indicators, the implementation procedure initiates with standardized processing of raw indicator data.

$$r_{ij} = \begin{cases} \dfrac{x_{ij} - x_{j,\min}}{x_{j,\max} - x_{j,\min}} & \text{The } j\text{−th indicator is a positive indicator} \\ \dfrac{x_{j,\max} - x_{ij}}{x_{j,\max} - x_{j,\min}} & \text{The } j\text{−th indicator is a negative indicator} \end{cases}, \tag{14}$$

where: x_{ij} is the original calculated value of the j-th evaluation index under the i-th working condition, $x_{\max}$ and $x_{\min}$ are the maximum and minimum values within the indicator dataset, and r_{ij} is the standardized value.

A normalized evaluation matrix was built for PFR performance assessment.

$$\boldsymbol{R} = \left(r_{ij}\right)_{mm} = \begin{bmatrix} r_{11} & r_{12} & \cdots & r_{1n} \\ r_{21} & r_{22} & \cdots & r_{2n} \\ \cdots & \cdots & \cdots & \cdots \\ r_{m1} & r_{m2} & \cdots & r_{mn} \end{bmatrix}. \tag{15}$$

Calculate the share p_{ij} of the i-th project under the j-th indicator based on the matrix $\boldsymbol{R}$:

$$p_{ij} = \frac{r_{ij}}{\sum_{i=1}^{m} r_{ij}} (0 \le r_{ij} \le 1). \tag{16}$$

To ensure numerical stability during logarithmic computations, it was necessary to ensure that the resulting $p_{ij} > 0$. For unsatisfied data, this can be calculated:

$$\widetilde{p}_{ij} = p_{ij} + a, \tag{17}$$

where a is the smaller constant that ensures that the resulting data is positive.

Then the entropy weight e_j was calculated for each indicator:

$$e_j = -k \sum_{i=1}^{n} p_{ij} \cdot \ln p_{ij}, \quad j = 1, 2, \cdots, n, \tag{18}$$

where the constant $k = \dfrac{1}{\ln m}$ and m is the number of samples used in this calculation.

The final calculated value of information value is:

$$d = 1 - e_j. \tag{19}$$

The information value d exhibited an inverse relationship with entropy weight e_j: lower d (indicating higher e_j) corresponded to reduced data dispersion for the indicator, signified diminished influence on the overall evaluation thus resulting in a lower weight; conversely, higher d increased the weight and vice versa similarly.

Finally, the entropy weight of each indicator was determined by the information utility value d. For comprehensive frequency regulation capability evaluation of the integrated renewable energy system, weights are calculated using all capability indicators to reflect their collective influence. Conversely, subsystem-specific evaluations (wind farm, photovoltaic, or energy storage) employed weights derived exclusively from their respective indicator sets. This hierarchical weighting approach ensures both system-wide and component-level assessments maintain objective prioritization based on data variability, where higher weights correspond to greater dispersion and systemic impact.

$$w_j = \frac{d_j}{\sum_{j=t_1}^{t_2} d_j}, \tag{20}$$

t_1–t_2 denoted the assigned indicators and w_j is the resulting entropy weight.

Following weight determination, the comprehensive PFR assessment index is synthesized through a linear weighting methodology.

$$G = \sum_{j=1}^{n} Awj, \tag{21}$$

where G is the final resulting capability index and A is the indicator score corresponding to the indicator weights.

The index is a dimensionless value in the range of [0, 1], calculated based on a unified global benchmark from all evaluation scenarios. The closer the value is to 1, the stronger the absolute comprehensive PFR capability of the wind-PV-storage system is, and the closer to 0, the weaker the absolute support capability for grid frequency stability is.

5. Case analysis and discussion

To validate the feasibility and effectiveness of the proposed PFR assessment framework, a wind-PV-storage coordinated frequency regulation simulation model was developed in MATLAB/Simulink (Fig. 1).

The test system operated at a 280 MW load level with synchronous generators configured with detailed prime mover, governor, and excitation system models. The renewable energy penetration rate of the system is approximately 30%. A 15 MW load step increase was introduced at 3 s to simulate power imbalance, thereby triggering synchronous generator rotor deceleration and system frequency decline, the system-related parameters are detailed in the appendix. This controlled disturbance enabled quantitative evaluation of the integrated renewable-storage system's frequency stabilization performance through dynamic response analysis.

5.1. Parameter configuration for diverse frequency regulation scenarios

To systematically evaluate the frequency regulation capability of wind, solar, and storage systems, this study categorized overall system performance into three scenarios from good to poor based on the performance scenarios of their relevant parameters. Additionally, while holding other parameters constant, the parameters for each energy source (wind, solar, storage) were independently tiered into four levels (optimal to suboptimal), yielding 15 distinct operational scenarios for comprehensive analysis.

First, the PFR of the integrated system was assessed across all 15 operational scenarios. Subsequently, the impacts of both systemwide parameter adjustments and individual subsystem parameter variations (wind, solar, or storage) on the frequency modulation metrics were analyzed. Finally, derived metrics were compared with the scenario parameters and the variance of frequency deviations to validate the assessment framework. Operational parameter configurations were systematically detailed in Table 1. The 15 cases are divided into 4 groups with a clear hierarchical structure: 3 benchmark multi-variable coupling cases (Scenarios 1–3), 4 wind turbine single-variable control cases (Scenarios 4–7), 4 photovoltaic single-variable control cases (Scenarios 8–11), and 4 energy storage single-variable control cases (Scenarios 12–15).

Table 1. System simulation parameters

Scenarios		J [kg·m^2]	$P_{\text{wind-ref}}$ [MW]	K_{w} [MW/Hz]	$P_{\text{pv-ref}}$ [MW]	K_{pv} [(MW/Hz)]
Overall	1	9 000	33.0	25	20.0	20
	2	6 000	36.5	20	22.0	15
	3	3 000	40.0	15	24.0	10
Wind	4	9 000	30.0	30	22.0	15
	5	7 200	33.0	25	22.0	15
	6	4 200	40.0	15	22.0	15
	7	3 000	43.0	10	22.0	15
Solar	8	6 000	36.5	20	18.0	25
	9	6 000	36.5	20	20.0	20
	10	6 000	36.5	20	24.0	10
	11	6 000	36.5	20	26.0	5
Storage	12	6 000	36.5	20	22.0	15
	13	6 000	36.5	20	22.0	15
	14	6 000	36.5	20	22.0	15
	15	6 000	36.5	20	22.0	15

Table continued on the next page

Table continued from the previous page

Scenarios		Energy storage reserve [Ah]	Initial soc [%]	K_b [MW/Hz]	Dead zone [Hz]		
					Wind	Solar	Storage
Overall	1	14.0	60	40	0.010	0.010	0.010
	2	10.0	55	30	0.020	0.020	0.020
	3	6.0	50	20	0.030	0.030	0.030
Wind	4	10.0	55	30	0.005	0.020	0.020
	5	10.0	55	30	0.010	0.020	0.020
	6	10.0	55	30	0.030	0.020	0.020
	7	10.0	55	30	0.050	0.020	0.020
Solar	8	10.0	55	30	0.020	0.005	0.020
	9	10.0	55	30	0.020	0.010	0.020
	10	10.0	55	30	0.020	0.030	0.020
	11	10.0	55	30	0.020	0.050	0.020
Storage	12	18.0	70	50	0.020	0.020	0.005
	13	14.0	60	40	0.020	0.020	0.010
	14	6.0	50	20	0.020	0.020	0.030
	15	2.0	40	10	0.020	0.020	0.050

This design adopts the classic control variable method, which can not only independently analyze the influence law of each core parameter of wind, photovoltaic and energy storage subsystems on the system's frequency regulation capability, but also verify the universality and discriminative power of the proposed evaluation framework under multi-variable coupling actual operating conditions.

To illustrate the impact of variations in the frequency regulation capabilities of individual subsystems within the wind-solar-storage system on the evaluation indices, this study implements a deloading operation. The wind farm and photovoltaic plant, initially operating under MPPT conditions with baseline outputs of 46 MW and 27.5 MW, are deloaded to operating ranges of 43 MW–30 MW and 26 MW–18 MW, respectively. Additionally, the capacity and initial SOC of the energy storage module are adjusted, alongside corresponding modifications to the droop coefficients and frequency deadbands of each subsystem. Modifying these parameters effectively alters the system's overall frequency regulation capability, thereby demonstrating the subsequent variations in the regulation evaluation indices.

Figure 4 reveals a direct correlation between the parameter optimization level in different scenarios (1–3) and the efficacy of renewable energy in providing primary frequency regulation power, which subsequently reduces the maximum frequency deviation.

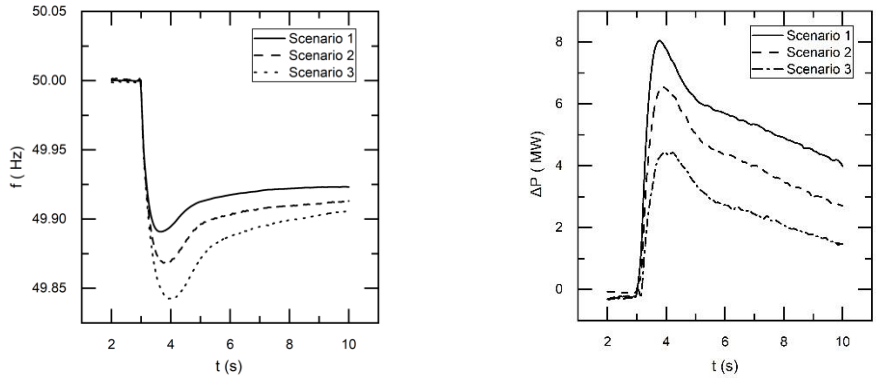

Fig. 4. System frequency response and renewable energy frequency regulation power output under Scenario 1–3: (a) system frequency dynamic curve; (b) total primary frequency regulation active power of the wind-solar-storage system

5.2. Computation of evaluation indicator

The simulation results for the various indicators set in Section 3 are shown in Table 2. Each column in Table 2 correspond to frequency modulation indicators C1–C10, with all indicators classified as benefit-type metrics where higher values indicate superior performance during load

Table 2. Evaluation results of each indicator

Scenarios		**C1 (J)**	**C2 (MW)**	**C3 (MW)**	**C4 (–)**	**C5 (MW)**
Overall	1	4 283	1.3110	1.4450	0.7837	7.5210
	2	3 252	9.5700	1.2370	0.7508	5.5250
	3	1 675	6.0890	0.9400	0.6734	3.5250
Wind	4	6 526	15.8900	2.2580	0.9346	5.5240
	5	4 647	13.0600	1.6330	0.7858	5.5250
	6	1 917	6.2460	0.6704	0.6027	5.5260
	7	1 022	3.0930	0.3980	0.5038	5.5220
Solar	8	2 875	9.5640	1.2200	0.7670	9.5160
	9	3 070	9.5840	1.1040	0.6959	7.5230
	10	3 443	9.6130	1.1570	0.6905	3.5290
	11	3 564	9.5910	1.3050	0.7536	1.5320
Storage	12	2 722	9.6150	1.0110	0.6558	5.5240
	13	2 982	9.5870	1.2480	0.7588	5.5260
	14	3 688	9.5050	1.3220	0.7605	5.5200
	15	4 027	9.5530	1.3980	0.7779	5.5230

Table continued on the next page

Table continued from the previous page

Scenarios		C6 (MW)	C7 (–)	C8 (Ah)	C9 (MW)	C10 (–)
Overall	1	1.4390	0.8286	3.9221	2.9940	0.8844
	2	1.1240	0.7521	2.5750	2.1100	0.8107
	3	0.7809	0.6957	1.4277	1.1090	0.7639
Wind	4	1.0550	0.7326	2.6100	1.9790	0.7951
	5	1.0930	0.7446	2.5915	2.0510	0.8042
	6	1.1530	0.7593	2.5631	2.1720	0.8162
	7	1.1670	0.7674	2.5440	2.2000	0.8224
Solar	8	2.0550	0.8972	2.6495	1.9310	0.7942
	9	1.6170	0.8470	2.5945	2.0200	0.8052
	10	0.6880	0.6553	2.5590	2.2020	0.8182
	11	0.2422	0.4288	2.5485	2.2380	0.8220
Storage	12	1.0250	0.7121	5.9139	3.4950	0.8882
	13	1.0880	0.7322	3.0555	2.6330	0.8499
	14	1.2140	0.7718	1.4466	2.6330	0.7423
	15	1.2910	0.7850	0.7802	2.6330	0.6067

increase and frequency decline scenarios. Through entropy weight method implementation, Table 3 presents the calculated entropy values (e_1–e_{10}) for each indicator. For the entropy weight method adopted in this study, the entropy value of an indicator directly reflects the dispersion degree of the indicator's data across all simulation working conditions. The smaller the entropy value, the higher the dispersion of the indicator data, the more effective information the indicator carries for distinguishing the frequency regulation capability of the wind-solar-storage system, and thus the higher weight will be assigned to this indicator.

Table 3. The calculated entropy values

e_1	e_2	e_3	e_4	e_5	e_6	e_7	e_8	e_9	e_{10}
0.9723	0.9813	0.9790	0.9968	0.9791	0.9753	0.9962	0.9687	0.9674	0.9988

It can be observed from Table 3 that indicators C1 (kinetic energy of wind turbine rotation), C8 (energy storage reserve) and C9 (energy storage frequency modulation energy contribution speed), yield the lowest entropy values. This demonstrates that these three indicators exhibit the most significant numerical variations under different operating conditions, and therefore hold the strongest discriminative power for the system's primary frequency regulation performance. In contrast, indicators with higher entropy values (e.g., C4 and C10) present lower data dispersion across all operating conditions, indicating that their performance remains stable under different operating scenarios, and thus they are assigned lower weights in the proposed evaluation framework.

Table 4 details the derived weight coefficients (w_1^1–w_{10}^1) obtained through comprehensive consideration of all C1–C10 indicators. This quantitative analysis establishes objective weight distributions reflecting the relative importance of each frequency regulation capability indicators in system performance evaluation.

$$D_1 = \sum_{j=1}^{n} r_{ij} w_j^1, \tag{22}$$

$$D_2 = \sum_{j=1}^{n} r_{ij} w_j^2. \tag{23}$$

Table 4. The calculated weight values

w_1^1	w_2^1	w_3^1	w_4^1	w_5^1	w_6^1	w_7^1	w_8^1	w_9^1	w_{10}^1
0.1497	0.1011	0.1130	0.0173	0.1130	0.1330	0.0205	0.1692	0.1768	0.0065

The results of the PFR capacity evaluation index D_1 for all scenarios all operating conditions are calculated by the linear weighting method based on Eq. 22, and the detailed results are listed in Table 5.

Table 5. The assessment result of the overall primary frequency regulation capacity of the system

Scenarios	**1**	**2**	**3**	**4**	**5**	**6**	**7**	**8**
D_1	0.6926	0.4745	0.2345	0.6707	0.5601	0.3771	0.3096	0.5874
Scenarios	9	10	11	12	13	14	15	
D_1	0.5236	0.4128	0.3583	0.6199	0.5095	0.4013	0.3535	

The evaluation results demonstrate strong consistency between parametric configurations and assessment result across all scenarios.

As shown in Table 5, scenarios 1–3 exhibited progressive degradation in primary frequency regulation capacity values (scenarios 1 > 2 > 3), which aligns with the variation trend observed in their parametric configurations and the frequency deviation characteristics depicted in Fig. 4. Scenarios 4–7, 8–11, and 12–15 corresponded to operational conditions where wind, solar, and storage parameters were adjusted individually while maintaining identical baseline settings. The evaluation results for these scenarios align consistently with their respective parameter configurations and the primary frequency regulation power they provide, as displayed in Fig. 5.

According to the entropy value in Table 3, the respective parameters of wind, photovoltaic and storage systems are assigned index weights as shown in Table 6. These weights are represented in a bar chart in Fig. 6, and they can be used to calculate the individually set PFR capability parameter D_2 for wind, PV and storage power sources as shown in Table 7. The calculation follows Eq. (23), where w_1^2–w_{10}^2 are the weight values calculated based on the entropy weights of the respective PFR indicators of wind, PV, and storage systems. In order to provide a more intuitive indication of the strength of the PFR capability, the variance E of the system frequency change for each scenario after normalisation was calculated as shown in Table 8.

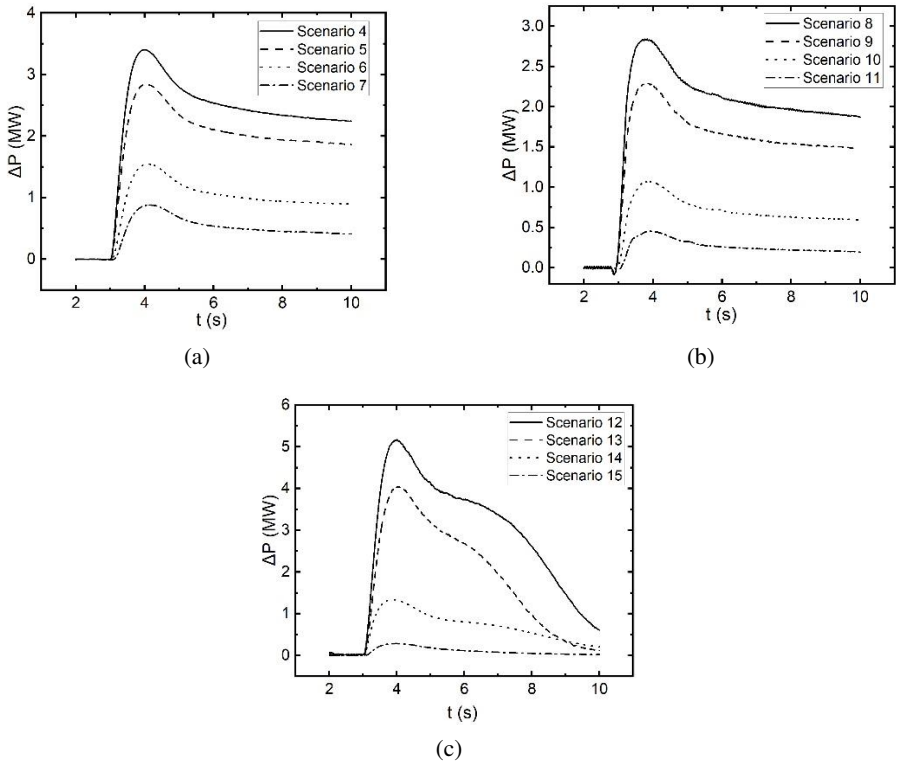

Fig. 5. PFR active power of the wind-solar-storage system in scenarios 4–15: (a) scenarios 4–7; (b) scenarios 8–11; (c) scenarios 12–15

Table 6. Subsystem-specific weight values for wind, solar, and storage systems

w_1^2	w_2^2	w_3^2	w_4^2	w_5^2	w_6^2	w_7^2	w_8^2	w_9^2	w_{10}^2
0.3929	0.2652	0.2965	0.0454	0.4239	0.4990	0.0771	0.4801	0.5015	0.0184

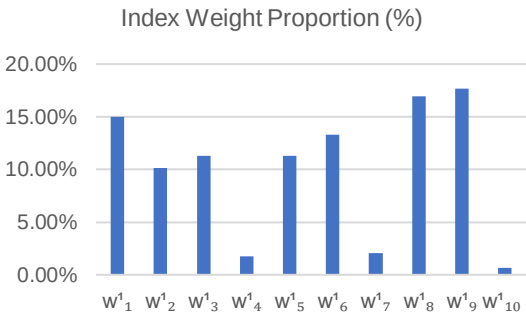

Fig. 6. The weights of each indicator calculated by the entropy weight method

Table 7. The evaluation results of PFR capability calculated separately by wind, solar, and storage systems

Scenarios	**Wind**				**Solar**				**Storage**			
	4	5	6	7	8	9	10	11	12	13	14	15
D_2	1.0000	0.6919	0.1831	0.0000	1.0000	0.7654	0.2660	0.0000	1.0000	0.5992	0.1957	0.0000

Table 8. Variance of frequency variation under different operating conditions

Scenarios	**1**	**2**	**3**	**4**	**5**	**6**	**7**	8
E	0.03139	0.04509	0.06363	0.03815	0.04200	0.04804	0.05149	0.03796
Scenarios	9	10	11	12	13	14	15	
E	0.04135	0.04890	0.05114	0.03234	0.03835	0.05359	0.61640	

The analysis of the variance E and the parameter configurations in Table 1 reveals that as the frequency modulation capability parameters degrade, the frequency deviation increases. Concurrently, both the overall PFR capacity assessment index D_1 and the individually set PFR capability assessment index D_2 exhibit corresponding declines. These findings confirm the validity of the entropy weight-based evaluation index of PFR in renewable energy systems.

5.3. Indicator sensitivity analysis and cross-system comparability of the evaluation framework

To quantify the impact of each evaluation indicator on the final composite evaluation results and validate the rationality and stability of the indicator system, this section employs the One-at-a-time (OAT) sensitivity analysis method. By sequentially removing individual indicators and recalculating the composite evaluation results, we determine the sensitivity level of each indicator by comparing the results before and after removal. the calculation formula is as follows:

$$\Delta_i = \frac{|I_{-I} - I_{\text{original}}|}{I_{\text{original}}} \times 100\%, \tag{24}$$

where: Δ_i is the sensitivity change rate of the i-th indicator C_i (in percentage); I_{-I} is the composite evaluation value recalculated with the remaining 9 indicators after removing the i-th indicator C_i; and I_{original} is the original composite evaluation value calculated based on all 10 indicators.

A larger sensitivity change rate indicates a higher impact of the indicator on the final evaluation result and stronger sensitivity. Based on the evaluation data of 15 typical operating conditions, we conducted sensitivity analysis on all 10 indicators, and the average sensitivity change rate of each indicator is shown in Table 9.

According to the results of sensitivity analysis, the extent to which each indicator influences the final evaluation outcome is directly correlated with the assigned weight coefficients (w_1^1–w_{10}^1). Indicators with higher weights – namely C9, C8, and C1 – demonstrate greater sensitivity. In contrast, indicators with lower weights, such as C7, C4, and C10, exhibit an average rate of

Table 9. Average sensitivity change rate of Indicators

Indicator	Average sensitivity change rate (%)	Sensitivity ranking
C9	8.85	1
C8	7.05	2
C1	6.63	3
C6	5.86	4
C3	4.24	5
C5	4.17	6
C2	3.08	7
C7	1.31	8
C4	0.67	9
C10	0.43	10

sensitivity variation below 2%. The sensitivity analysis further reveals that core performance metrics, including the response speed and frequency regulation speed of energy storage systems, along with the spinning reserve capacity of wind power – due to their relatively high weighting – possess pronounced sensitivity. This outcome aligns with the underlying design logic of the indicator system and validates the appropriateness of the indicator selection.

For cross-system performance comparison between different wind-PV-storage hybrid systems, the proposed framework enables reliable and objective comparability through a standardized calculation process: the operating indicator data of all evaluated systems are integrated into a unified dataset, followed by consistent data normalization and holistic entropy weight calculation for the full dataset. The entropy-based weighting scheme has natural adaptability to grid dispatch-oriented cross-system evaluation: it automatically assigns higher weights to core indicators that determine the absolute frequency support capability (e.g., frequency regulation reserve capacity, Frequency Modulation Energy Contribution Speed), which is fully aligned with the practical demand of power grid operation. It should be clarified that fixed weight coefficients derived from a single system are not recommended for direct cross-system application, to avoid evaluation distortion caused by essential parameter differences between heterogeneous systems.

5.4. Discussion

To further verify the effectiveness and advancement of the proposed evaluation index system, a systematic comparative analysis with two representative state-of-the-art studies in this field, as well as traditional dynamic frequency performance metrics, was conducted. First, compared with traditional dynamic frequency performance metrics (such as frequency nadir, rate of change of frequency (RoCoF), and frequency recovery time), the proposed index system has unique advantages: it has predictive evaluation capability – traditional frequency metrics can only reflect the post-disturbance frequency response results, while our index can evaluate the inherent frequency regulation capability of the wind-solar-storage system before frequency disturbances occur, providing proactive guidance for grid dispatch and operation; it supports subsystem-level analysis – traditional metrics can only reflect the overall frequency performance of the entire

power system, but our index can independently evaluate the frequency regulation performance of wind, photovoltaic, and energy storage subsystems separately, enabling precise positioning of the advantages and shortcomings of each power source's frequency regulation performance; it has strong independence from external interference – traditional frequency metrics are easily affected by other components in the power system such as synchronous generators, while our index solely focuses on the wind-solar-storage system's own performance indicators, ensuring an objective and independent evaluation of the renewable energy system's frequency regulation capability without interference from external frequency regulation entities. Compared with the wind-storage binary system-oriented evaluation framework proposed by Hao *et al*. [25], the index system in this paper fully covers the frequency regulation characteristics of wind, photovoltaic and energy storage subsystems, which is more consistent with the mainstream grid-connected wind-solar-storage hybrid engineering scenarios, and the multi-dimensional index system with 10 core indicators avoids the one-sidedness of single-dimensional evaluation. In contrast to the multiple linear regression-based frequency stability assessment method proposed by Lim *et al*. [26], the entropy weight-based objective weighting mode adopted in this study thoroughly eliminates the subjective randomness of equal weight setting and the strong dependence on preset scenarios of linear regression, with better objectivity, robustness and dynamic adaptability to complex grid operating conditions.

Despite the above advantages, the framework still has limitations in practical application. First, the weight calculation has a certain dependence on the working condition coverage of the input dataset, and insufficient extreme operating condition data will affect the stability of evaluation results. Second, the current index system focuses on the technical performance of frequency regulation, without incorporating full-life-cycle economic indicators of frequency regulation services. Third, the system does not include the frequency regulation contribution of synchronous generators and other auxiliary frequency regulation equipment, so its evaluation performance for large power grids with multiple types of frequency regulation entities needs to be improved.

6. Conclusions and future work

This study systematically analyzes the primary frequency regulation mechanisms and dynamic response characteristics of wind turbines, photovoltaic systems and electrochemical energy storage, targeting the frequency stability challenges in high-renewable-penetration power systems. On this basis, a primary frequency response evaluation framework for wind-solar-storage hybrid systems based on the entropy weight method is proposed, which fully integrates the frequency regulation characteristics of each component. The results verify that the proposed framework can accurately quantify the frequency regulation performance of wind-solar-storage systems under diverse operating conditions and identify the performance shortcomings of each subsystem, which has important engineering value for enhancing the primary frequency regulation support capacity of renewable energy stations and ensuring the safe operation of high-renewable-penetration power grids.

Future work will be carried out in the following aspects: enrich the extreme operating condition dataset and introduce robust optimization to improve the stability of weight calculation; incorporate full-life-cycle economic indicators to build a techno-economic coupled evaluation framework; supplement the evaluation indicators of conventional and new auxiliary frequency regulation equipment, to build a comprehensive evaluation system covering all types of frequency regulation entities and further expand the application scope of the framework.

Appendix

Table A.1. System parameter configuration

Simulation module	Parameter	Symbol	Value	Unit
Synchronous generator	Rated capacity	S_b	200	MW
	Generator inertia constant	H	4	s
	Governor speed droop	R_s	0.02	pu
	Speed relay time constant	T_{sr}	0.001	s
	Servo-motor time constant	T_{sm}	0.05	s
	High-pressure turbine time constant	T_3	10	s
	Reheater time constant	T_4	3.3	s
	Intermediate/low-pressure turbine time constant	T_5	0.5	s
	Rated speed	ω_{nom}	3 600	rpm
Permanent magnet direct-drive wind turbine	Rated power	S_{wind}	996	kW
	Rotor diameter	D	50.5	m
	Rated wind speed	V_{rated}	12	m/s
	Wind speed	V_{wind}	11	m/s
	Rated rotational speed	ω_{rated}	3.81	rad/s
Photovoltaic system	Open-circuit voltage	V_{oc}	430	V
	Temperature coefficient of V_{oc}	α	0.015	%/°C
	Temperature coefficient of I_{sc}	β	–0.1	%/°C
	Short-circuit current	I_{sc}	20	A
	Series resistance	R_s	2.2	Ω
	Number of cells in series	N_s	3	–
	Number of parallel modules	N_p	1200	–
	PV module temperature	T_{amb}	25	°C
	Solar irradiance	G	1 000	W/m^2
Battery	Rated voltage	V_{bat}	500	V
	Internal resistance	R_{bat}	0.5	Ω
	Response time	T_b	20	s
	Operational SOC range	SOC	20%–90%	–

Acknowledgements

This work was supported by the Henan Province Science and Technology Research Project (No. 252102241060), the Training Plan for Young Backbone Teachers in Undergraduate Universities in Henan Province (No. 2023GGJS087), and the Henan Provincial University Scientific and Technological Innovation Team (No. 26IRTSTHN037).

References

[1] Yin Y., Liu T., Wu L., He C., Liu Y., *Frequency-constrained multi-source power system scheduling against N-1 contingency and renewable uncertainty*, Energy, vol. 216, 119296 (2021), DOI: 10.1016/j.energy.2020.119296.

[2] Greenwood D.M., Lim K.Y., Patsios C., Lyons P.F., Lim Y.S., Taylor P.C., *Frequency response services designed for energy storage*, Applied Energy, vol. 203, pp. 115–127 (2017), DOI: 10.1016/j.apenergy.2017.06.046.

[3] Knap V., Chaudhary S.K., Stroe D.I., Swierczynski M., Craciun B.I., Teodorescu R., *Sizing of an energy storage system for grid inertial response and primary frequency reserve*, IEEE Transactions on Power Systems, vol. 31, no. 5, pp. 3447–3456 (2015), DOI: 10.1109/TPWRS.2015.2503565.

[4] Bevrani H., Golpîra H., Messina A.R., Hatziargyriou N., Milano F., Ise T., *Power system frequency control: An updated review of current solutions and new challenges*, Electric Power Systems Research, vol. 194, pp. 107–114 (2021), DOI: 10.1016/j.epsr.2021.107114.

[5] Lv C., Xu Y., Wu X., Zhang Q., *Characteristic analysis and optimal regulation of primary frequency regulation condition in low water head area based on hydraulic-mechanical-electrical coupling model of pumped storage unit*, Complexity (2020), DOI: 10.1155/2020/6161784.

[6] Kumar R.K., Choudhary J., *Design of a novel control scheme for the operation of the doubly fed induction generator*, Archives of Electrical Engineering, vol. 73, no. 2, pp. 373–392 (2024), DOI: 10.24425/aee.2024.149922.

[7] Zhang B., Ping S., Long Y., Jiao Y., Wu B., *Virtual synchronous generator frequency response study of energy computing and storage devices*, Archives of Electrical Engineering, vol. 71, no. 4, pp. 895−907 (2022), DOI: 10.24425/aee.2022.142115.

[8] Wu X., Jiang W., Zhaowei L., Huang H., Zhu S., Zhu X., *Study on the Improved Evaluation Method of Primary Frequency Modulation for Grid-connected Units*, In IOP Conference Series: Earth and Environmental Science, vol. 223, no. 1, pp. 12–37 (2019), DOI: 10.1088/1755-1315/223/1/012037.

[9] Maihemuti S., Wang W., Wu J., Wang H., *New energy power system operation security evaluation based on the SWOT analysis*, Scientific reports, vol. 12, no. 1 (2022), DOI: 10.1038/s41598-022-16444-4.

[10] Li S., Wang Y., *Dynamic performance assessment of primary frequency modulation for a power control system based on MATLAB*, Processes, vol. 7, no. 1, 11 (2018), DOI: 10.3390/pr7010011.

[11] Zhang Y., Tang F., Liang X., Sun J., Li H., Ru H., *Prediction method of primary frequency modulation capability of power system based on MEA-BP algorithm*, Energy Reports, vol. 9, pp. 111−118 (2023), DOI: 10.1016/j.egyr.2023.04.291.

[12] Rakhshani E., Gusain D., Sewdien V., Torres J.L.R., Van Der Meijden M.A., *A key performance indicator to assess the frequency stability of wind generation dominated power system*, IEEE Access, vol. 7, pp. 130957–130969 (2019), DOI: 10.1109/ACCESS.2019.2940648.

[13] Chi C., Zhao H., Han J., *Study on quantitative evaluation index of power system frequency response capability*, Energies, vol. 15, no. 24, 9423 (2022), DOI: 10.3390/EN15249423.

[14] Wang Y., Zhao D., Yin J., Yang M., *An interconnected power grid active power control performance evaluation method considering energy storage frequency modulation*, In 2018 2nd IEEE Conference on Energy Internet and Energy System Integration (EI2), pp. 1–6 (2018).

[15] Xudong L., Hua L., Weichen X., Jiliang J., Ziyue C., *Research on primary frequency regulation performance index system of new energy station*, 2024 IEEE 6th Advanced Information Management, Communicates, Electronic and Automation Control Conference (IMCEC), vol. 6, pp. 11–15 (2024).

[16] Li S., Cao Z., Hu K., Chen D., *Performance assessment for primary frequency regulation of variable-speed pumped storage plant in isolated power systems*, Energies, vol. 16, no. 3, 1238 (2023), DOI: 10.3390/EN16031238.

[17] Shi Q., Wang G., Ma W., Fu L., Wu Y., Xing P., *Coordinated virtual inertia control strategy for D-PMSG considering frequency regulation ability*, Journal of Electrical Engineering and Technology, vol. 11, no. 6, pp. 1556–1570 (2016), DOI: 10.5370/JEET.2016.11.6.1556.

[18] Li C., Zhang Z., Li J., Ma Y., Zou J., *Design of control strategy and effect evaluation for primary frequency regulation of wind storage system*, Frontiers in Energy Research, vol. 9 (2021), DOI: 10.3389/FENRG.2021.739439.

[19] Li Z., Yang L., Zhou W., Li C., *Active frequency support capability evaluation of photovoltaic stations based on bi-level evaluation method*, Scientific Reports, vol. 15, no. 1 (2025), DOI: 10.1038/S41598-025-88428-Z.

[20] Meng L., Zafar J., Khadem S.K., Collinson A., Murchie K.C., Coffele F., Burt G.M., *Fast frequency response from energy storage systems – a review of grid standards, projects and technical issues*, IEEE transactions on smart grid, vol. 11, no. 2, pp. 1566–1581 (2019), DOI: 10.1109/tsg.2019.2940173.

[21] Shu H., Wang G., Chen J., Ma H., He T., *Coordinated control of wind-storage combined with primary frequency regulation and variable coefficient based on wind speed and SOC*, Journal of Energy Storage, vol. 87 (2024), DOI: 10.1016/j.est.2024.111356.

[22] Xueyang Z., Zhang C., Shunliang W., *Primary frequency control of wind turbine based on deloading coefficient variation*, Electric Power Automation Equipment, vol. 42, no. 8, pp. 119–125 (2022), DOI: 10.16081/j.epae.202204061.

[23] Wu Q., Song X., Zhang J., Yu H., Huang J., Dai H., Luo H., *Study on self-adaptation comprehensive strategy of battery energy storage in primary frequency regulation of power grid*, Power System Technology, vol. 44, no. 10, pp. 3829–3836 (2020), DOI: 10.13335/j.1000-3673.pst.2019.1214.

[24] Lijun W., Xiaomin L., *The Optimization of Coordinated Control System Under AGC Mode for Supercritical Generation Unit Based on "Two Documents"*, Modern Electric Power, vol. 31, no. 5, pp. 84−89 (2011), DOI: 10.19725/j.cnki.1007-2322.2011.02.017.

[25] Hao J., Zheng H., Cheng X., Li Y., Bo L., Wei J., *Optimal Control Strategy and Evaluation Framework for Frequency Response of Combined Wind–Storage Systems*, Technologies, vol. 13, no. 6, 259 (2025), DOI: 10.3390/technologies13060259.

[26] Lim S., Seo K., Park J.W., Lee K.Y., *New frequency stability assessment based on contribution rates of wind power plants*, International Journal of Electrical Power & Energy Systems, vol. 164 (2025), DOI: 10.1016/j.ijepes.2024.110388.